

Characterization techniques employed in the study of niobium and tantalum-containing materials

Maria Ziolk^{*}, Izabela Nowak

Faculty of Chemistry, A. Mickiewicz University, Grunwaldzka 6, PL-60-780 Poznan, Poland

Abstract

This paper summarizes the techniques applied for the characterization of niobium and tantalum species in solid materials and described in the literature in the last two decades. The idea of this paper is not only the exhibition of new and developed techniques but also pointing at the papers in which readers can find the particular results of the applied methods.

© 2002 Elsevier Science B.V. All rights reserved.

Keywords: Niobium-, tantalum-containing compounds; Characterization techniques

1. Introduction

The development in the niobium and tantalum chemistry in the last decades was possible, thanks to a great progress in the spectroscopic and other physical methods used for the characterization of solids.

The new analytical techniques and the new application of well known methods used for Nb and Ta identification and characterization in the last years will be described in this paper wider, whereas, the other methods will be mentioned and/or classify only. Characterization of Nb- and Ta-containing compounds covers the following features:

1. Metal content.
2. Structure and texture of solids.
3. Surface state of solids.

2. Metal content [1–10]

The separation of niobium and tantalum from other elements and from each other has been one of the most complex problems faced by analytical chemistry. Both of these elements tend to partition between the filtrate and the precipitate, no matter which precipitant is used. The development of new techniques based on ion exchange (solid and liquid exchangers) and liquid–liquid extraction has simplified the separation of niobium and tantalum. These techniques take advantage of the fact that both elements and associated ones can exist in solution as characteristic complex species with significant differences in distribution coefficients and relative stabilities. Liquid surfactant membranes impregnated with octanol as a carrier medium have been used for the separation of Nb and Ta [1]. Ion-interaction reverse-phase high-pressure liquid chromatography (RP-HPLC) has been recently applied with reasonable success for determination of Nb and Ta [9,10]. These methods

^{*} Corresponding author. Tel.: +48-61-8291243;
fax: +48-61-8658008.
E-mail address: ziolk@amu.edu.pl (M. Ziolk).

relied upon separation of anionic ternary complexes of Nb(V) and Ta(V) using various metallochromic ligands, including 4-(2-pyridylazo)resorcinol (PAR), 2-(5-bromo-2-pyridylazo)-5-diethylaminophenol (Br-PADAP), and 2-(5-bromo-2-pyridylazo)-5-[*N*-propyl-*N*-(3-sulfopropyl)amino]-phenol (Br-PAPS). The complexes were separated on a C18 column dynamically coated with tetrabutylammonium hydroxide [4]. Recently, separation of Nb(V) and Ta(V) as ternary complexes with citrate and metallochromic ligands by capillary electrophoresis has been proposed [4].

Since chemical detection and identification tests for niobium and tantalum generally require prior removal of most accompanying elements, the preferred methods for detection and identification are spectroscopic. The intensities of niobium atomic emission lines in the arc spectrum depend largely on the type of excitation and exceed those of tantalum lines by a factor of about 10. It is possible to detect 0.05% niobium in the material by a spark technique [9].

X-ray fluorescence spectrometry is also an excellent tool for the detection of both niobium and tantalum, and with somewhat better sensitivity than arc or spark spectroscopy. Here also the intensity of niobium radiation is considerably greater than that of tantalum [1,2].

Spectrophotometric methods are based on the formation of colored complexes with inorganic or organic reagents. These methods, generally, have the advantage that they are rapid, require only a minimum amount of preliminary separation from most accompanying elements and in some cases are capable of differentiating between niobium and tantalum [1]. As an example, color development between *o*-hydroxyhydroquinonephthalein and niobium or tantalum has been used in the presence of hexadecyltrimethylammonium chloride (HTAC) in strong acidic media [3].

Nb(V) and Ta(V) can also be determined using inductively coupled plasma-mass spectrometry (ICP-MS) [5,6] and inductively coupled plasma-atomic emission spectrometry (ICP-AES) [7,8].

3. Structure and texture of solids

Techniques often used for structure (including bulk phase structure) and texture (surface area, particle size,

porosity, pore size distribution, pore volume, radius) characterization include the methods described below.

3.1. Gas adsorption

Nitrogen adsorption isotherms are commonly used for the estimation of surface areas and pore size distribution, pore volume and radius in solids and have been also widely applied to the study of Ta- and Nb-containing compounds [11–17].

3.2. Electron microscopy

Scanning electron microscopy (SEM), transmission electron microscopy (TEM), or high-resolution TEM (HRTEM) provide direct visual information on the size, shape, dispersion and morphology of solids. Some examples of their application are shown below [18]. Structural changes in Ta₂O₅ were studied using SEM [19]. This technique was also applied to the characterization of the nanostructure of Nb₂O₅ [20] and Nb-oxide deposited on Pt [21], as well as to the surface morphology of oxidized Nb-implanted Ti and Ti–4Nb mixture [22]. SEM micrographs of Nb₂O₅ films treated at various temperatures allowed the observation of a temperature transformation of the amorphous niobium gel into crystalline particles [23]. SEM study of calcined tantalum silicalite (TaS-1) indicated that variation of the Ta content does not lead to significant modification of its morphology, and moreover, a TEM image revealed the absence of amorphous matter outside the crystals of this material [24]. The microstructural stability of Cu–Nb microcomposite wires fabricated by the bundling and drawing process has been examined using TEM [25].

High-resolution electron microscopy (HREM) studies have demonstrated that lattice-imaging techniques can provide atomic scale information in complex oxides or other solids. Recently, Sayagués and Hutchison [26,27] have developed a new technique, controlled environment transmission electron microscopy (CETEM), and applied it to niobium oxides. This method is a combination of a gas reaction cell (GRC, also designated as an environmental cell) and a high-resolution transmission electron microscope. This technique allows real-time observation of structural changes at the atomic level. In a GRC installed in a HRTEM, samples can be manipulated in an ambient

atmosphere ($p < 50$ mbar). This arrangement permits not only the observation of solid–gas reactions in situ at close to the atomic level but also the induction of structural modifications under the influence of a plasma, generated by ionization of gas particles by an intense electron beam [28]. Solid state reactions of non-stoichiometric niobium oxides and niobium tungsten oxides with different gases (O_2 , H_2 , and He) have been studied by Sayagués et al. [28,29]. GRC micrographs and the corresponding electron diffraction patterns (EDP) of $Nb_{12}O_{29}$ treated under vacuum, with oxygen and with hydrogen showed that the Nb-oxide structure is changed after the oxidation indicating the formation of a superstructure. One set corresponded to $Nb_{12}O_{29}$ and the other to a $Nb_{10}O_{25}$ structure. The original structure of $Nb_{12}O_{29}$ was rebuilt after the reduction with hydrogen.

3.3. X-ray techniques

X-ray diffraction (XRD) is mostly used for bulk structure analysis and it is suitable for size determination, if the concentration of the component of interest is high enough. XRD patterns of various Nb- and Ta-containing compounds are shown in many papers. It is useful technique for differentiate niobium pentoxide from tantalum pentoxide [30]. Two forms of Ta_2O_5 (hexagonal δ - Ta_2O_5 and orthorhombic β - Ta_2O_5) were characterized with XRD patterns [19]. Nb_2O_5 films coating various matrices have been studied [23,31–33], as have changes in Nb_2O_5 resulting from calcination at various temperatures [34]. XRD has been applied also to the detection of solid state interaction between Nb or Ta compounds and other solids. Formation of new phases can be detected in the Co/ Nb_2O_5 system [35], Ni- Nb_2O_5 /SiO₂ material [36], NbNaY zeolite [37], and Cu-NbMCM-41 mesoporous molecular sieves [38]. Solid state interactions can be also estimated on the basis of Nb_2O_5 phase disappearance observed, for example, during in situ XRD study of Nb_2O_5 and HNaY zeolite mixtures heated at various temperatures [39].

Time resolved diffractograms were used to observe structural evolution of Nb and Al during combustion leading to the formation of a new compound, $NbAl_3$ [40]. Niobium nitride films were well defined by XRD patterns [41], and metal Nb [42] and Nb–H, Nb–N systems [43] have been characterized. The XRD

pattern of TaS-1 [24] and of NaCl–KCl– K_2NbF_7 , NaCl–KCl– K_3NbOF_6 , NaCl–KCl– $K_3NbO_2F_4$ [44] have been reported. In addition, oxide phases have been assigned in Mo–V–Sb–Nb–O bulk materials [45] and in Nb-alloys and Nb sulfides [46].

XRD is generally applied to the investigation of crystalline solids. However, the ordered amorphous mesoporous materials, like NbMCM-41 [47,48], or mesoporous tantalum and niobium oxides [49,50] can be characterized with XRD at a low-angle range.

The position-sensitive X-ray detection (CPSD) method allowed the measurement of the equation of tantalum state [51]. Glancing angle X-ray diffraction (GAXRD) measurements were performed in order to obtain the TaO film composition [52] and also were applied to the study of Ti–4Nb system [22]. This system has been also studied with energy dispersive X-ray (EDX) spectroscopy [22]. The composition of $(Nb_{1-x}Ta_x)_2O_5$ films was checked by EDX [53]. The EDX analysis demonstrated the homogeneous distribution of Ni, Mo, and Nb in the hydrotreating NiMo catalysts doped with Nb sulfide [54]. The EDX technique combined with STEM allowed the analysis of V, Nb, and P in VPO and NbPO materials depending on the different morphologies observed by SEM [55]. TEM–EDX analysis provides high spatially resolved insight about the distribution of niobium in Nb-doped TiO₂ thick film [56].

3.4. Temperature programmed methods

Differential thermal analysis (DTA) and thermal gravimetric analysis (TGA) are very useful in the study of solid phase structure. The first measures energy changes as the sample is scanned through phase changes; the second records weight loss or gain. Additional information can be obtained using reactive atmosphere, usually hydrogen. With hydrogen, the technique called temperature programmed reduction (TPR) gives information on the reducibility of oxides [57]. TG/DTA analysis was applied to the study of the crystallization of Nb-oxides deposited on various matrices (Pt [21], ITO-glass [23,31]) and sodium tetraperoxo niobate [58].

H_2 -TPR study allows distinguishing between Nb in the framework (high temperature peak) and extra framework (low temperature peak) positions in the mesoporous molecular sieves of MCM-41 type [59].

This technique is also useful for the estimation of the interaction between niobium in a matrix and supported transition metal (for instance Cu [38], Ni [60], Mo [61]).

3.5. Infrared and Raman spectroscopy

The knowledge of the crystal chemistry of solids is largely based on the results of infrared (IR) and Raman spectroscopy. These methods are also useful in the study of amorphous materials although the bands are not so intensive as for the crystal phases.

In the so-called “skeletal region” ($300\text{--}1300\text{ cm}^{-1}$) the lattice vibrations can be observed. IR spectra in the skeletal region of Nb-containing compounds are reported in many papers (as examples [23,34,44,59,62–65]), whereas that of TaS-1 is shown by Ko and Ahn [24]. Generally, in the range of $600\text{--}950\text{ cm}^{-1}$ the Nb–O stretching vibrations can be observed [23]. The IR band near 920 cm^{-1} is assigned to the stretching mode of Nb=O bonds while the stronger one near 620 cm^{-1} was assigned to the stretching of longer bridging Nb–O–Nb bonds in the distorted NbO₆ octahedra [64]. The IR spectroscopy allowed the identification of both NbO₆ distorted octahedra and tetrahedral orthophosphate species present in the bulk crystalline NbPO₅ when niobic acid was impregnated with phosphoric acid [64]. IR spectra in the Nb–O and Ta–O stretching region strongly depend on the composition and structure of the materials containing metal–oxygen bonds. Zhou and Andrews [65] developed the knowledge in this area, thanks to the production of MO, MO₂, MO₂[−], and MO₂⁺ (where M = Ta or Nb), via the reaction of laser-ablated niobium and tantalum atoms with oxygen and IR spectroscopy study of these molecules. The IR band at about 960 cm^{-1} is often used as evidence for the incorporation of metal into the siliceous skeletal of molecular sieves, and so interpretation, one can find also for Nb and Ta silicalites [24,66,67]. However, the literature proposes various interpretation of the origin of this band [68–70] and now it is generally accepted that the band at $\sim 960\text{ cm}^{-1}$ is due to a Si–O vibrational mode perturbed by the presence of metal ions in a neighboring position.

Some aspects of the crystal chemistry of niobium and tantalum complex oxides with a perovskite-type structure have been considered on the basis of the

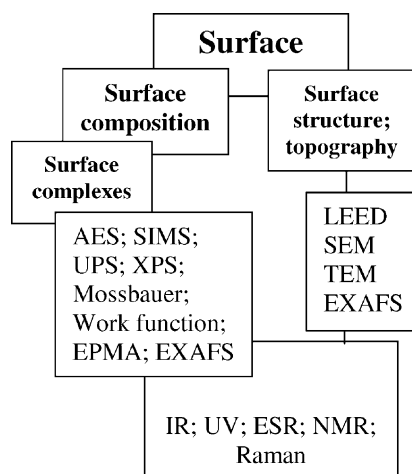
vibrational spectroscopy methods (IR absorption and spontaneous Raman scattering) [71].

Raman spectroscopy applied for the characterization of bulk Nb and Ta oxides is reported in Section 4.3 together with the characterization of surface properties.

4. Surface state of solids

The characterization of the surface state includes surface composition, complexes, structure and topography. The methods commonly used for that characterization are well illustrated by the diagram presented in Scheme 1 adapted from Ref. [18,72].

Most of the methods presented in Scheme 1 have been already applied to the characterization of niobium- and tantalum-containing compounds. However, some of them are difficult or impossible to be used for Nb or Ta compounds. There are no literature data showing ⁹³Nb MAS NMR spectra of solids containing niobium. It is due to a high niobium spin nuclei ($\frac{9}{2}$) which make difficult to obtain a good quality NMR spectrum. Recently, Shore and coworkers [73] applied pure-phase two-dimensional NMR spectroscopy which allowed the determination of the quadrupolar coupling constants of the niobium sites in lead metaniobate (PbNb₂O₆) and lead magnesium niobate (Pb(Mg_{1/3}Nb_{2/3})O₃) solid-solutions. The



Scheme 1. Methods available for the characterization of surface state of nanoclusters, adapted from Ref. [18].

^{93}Nb nutation spectra of both compounds are shown in their paper.

4.1. Microscopy analyses

Generally, microscopy techniques described in the previous section are well adapted to the characterization of the surface structure of solids.

A relatively new method, not shown in the diagram, is scanning tunneling microscopy (STM), which has particularly great potential for in situ chemical studies [74]. It can provide real-space images of surfaces of conducting materials down to the atomic scale. The operation of STM is surprisingly simple. In contrast to other electron microscopies and surface analytical techniques using electrons, STM can be operated in air, liquids, vacuum and reaction conditions because there are no free electrons involved in the STM experiments. Following the invention of the STM in 1981 [75], the surface structures of several transition metal oxides have been studied by the use of STM. A serious limitation of the STM technique so far is its lack of chemical sensitivity.

STM makes possible the determination of a nanoclusters, including the stabilizing ligand shell and it is an effective probe of the electronic properties of such nanoparticles [18]. For instance, STM observation of single NbO nano-crystal revealed that the entire surface is covered by small protrusions having a pyramid shape with a flat top [76].

4.2. X-ray photoelectron spectroscopy (XPS)

XPS technique is widely applied method to the study of a chemical composition of solid surfaces. It allows also the investigation of the in-depth distribution of the different compounds. Daccà et al. [77] used XPS method for the deep study of Nb samples, including metallic niobium, various niobium oxides and niobium carbide. They measured XPS and ARXPS (angle resolved XPS) spectra in the temperature range between room temperature and 1273 K. The authors performed an angularly resolved analysis that allows the evaluation of the thickness of the compounds present on the surface. Work function values, ϕ , was obtained by measuring the total width of the photoelectron spectrum. Alternating XPS spectra and

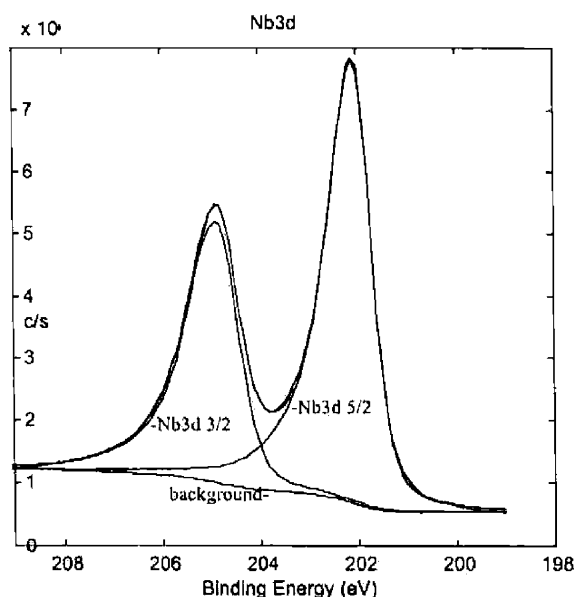


Fig. 1. Deconvolution of the Nb 3d doublet: the line shape is reproduced by two Gaussian–Lorentzian curves, that represent the Nb doublet, and by the background [77].

ϕ measurements with ion sputtering (Ar^+ at 2 keV) performed depth profile analysis.

Generally, niobium in various compounds gives rise to the Nb 3d doublet ($3d_{3/2}$ and $3d_{5/2}$) in the XPS spectrum as shown, for example in Fig. 1. The binding energy (BE) and the intensity of each XPS line depend on various factors. With the decrease of the oxidation state of niobium the position of XPS peaks shifts to a lower BE. Sugiyama et al. [78] prepared various niobium oxides using a microwave plasma heating method and they observed the following niobium species characterized by XPS lines: Nb^{5+} (207.4, 209.7 eV); Nb^{4+} (205.0, 207.0 eV), and Nb^{2+} (204.4, 206.3 eV) for $3d_{5/2}$ and $3d_{3/2}$, respectively. Niobia (Nb_2O_5) films described in [33] represents in XPS spectrum a pair of peaks due to Nb $3d_{3/2}$ and $3d_{5/2}$ core levels at the binding energies of 210.1 and 207.3 eV, respectively (the same values were observed for Nb_2O_5 doped TiO_2 thin films [79]). After lithiation, the peaks due to Nb $3d_{3/2}$ and $3d_{5/2}$ were observed at 209.8 and 207.0 eV indicating the partial reduction of Nb^{5+} according to



XPS studies of mesoporous niobium(V) oxide treated with potassium fulleride (K_3C_{60}) [49,50] displayed a niobium $3d_{5/2}$ emission at 207.1 eV, i.e., almost 1 eV lower than that of the parent mesoporous niobium oxide. It is consistent with the reduction of the walls to an oxidation state of ca. 4.4+. The Nb 3d peak positions can be readily used to deduce the mean oxidation state of the Nb walls in mesoporous oxides. Antonelli and coworkers [80] demonstrated that with increasing alkali metal (used for the reduction of Nb-oxide) size the XPS peaks are moved to a lower BE.

The higher BE of Nb $3d_{5/2}$ = 207.9 eV in niobosilica mesoporous molecular sieve, NbMCM-41 [38], than that in Nb_2O_5 indicates the interaction of Nb with Si, both located in the skeletal of the molecular sieve. The introduction of Cu into this matrix shifts the BE of Nb $3d_{5/2}$ to the higher value (208.1 eV) suggesting the additional effect of polarization by Cu species. The literature shows the XPS spectra of Nb_2O_5 interacting with various metals, for instance Ni [36], Co [81], Pd [54]. The transformation of Nb_2O_5 into NbC leads to the decrease of BE from 209.8 and 207.1 to 205.2 and 202.5 eV [82]. The XPS binding energies of Nb 3d in niobium nitrides are also lower than that in oxides and depend on the matrix on which the nitrides are deposited [41].

The intensity of the photoelectron peaks depends on the density of niobium species. The decrease in their intensity after treating of uranium-based alloy (U–14.1 at.% Nb) with oxygen can be interpreted as a result of the diffusion of niobium into the bulk or lowering of the Nb surface density due to the formation of oxide [83]. The intensities of XPS lines are used for the calculation of the composition of the surface. For example niobium(V) and tantalum(V) oxides coated by monolayers of dodecyl phosphate and 12-hydroxy dodecyl phosphate were analyzed by XPS technique [84]. Normalized XPS intensities of C 1s, O 1s, Ta 4f, Nb 3d and P 2p divided by the corresponding elemental sensitivity factors and normalized to 100% allow the determining of the composition of these materials.

The XPS spectra of potassium tantalate niobate are discussed in [85] and that of LiNbO_3 in [86]. Ta 4f spectra of amorphous Ni–30Ta–3Ir alloy are shown in [87].

Tantalum $4f_{7/2}$ and $4f_{5/2}$ emissions are in the region ca. 27 and 29 eV, respectively. The mesoporous tantalum(V) oxide exhibits two peaks in XPS spectrum at

26.5 and 28.2 eV for Ta $4f_{7/2}$ and $4f_{5/2}$, respectively [49]. These values decrease when tantalum(V) oxide is treated with K_3C_{60} indicating the reduction of Ta.

Recently, Wachs et al. [88] applied XPS for the estimation of Ta density on the different supports at monolayer surface coverage. They have found 5.6, 5.9, 6.0, and 2.1 Ta atoms/nm² for Al_2O_3 , TiO_2 , ZrO_2 , and SiO_2 applied as supports, respectively.

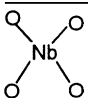
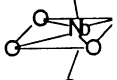
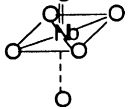
4.3. Raman spectroscopy

Raman spectroscopy primarily provides information on the vibrational properties of a bulk oxide. Typically, Raman spectroscopy analyses to a depth of 1 μm into the surface of a solid [45,89]. Amorphous materials give weak Raman spectra. Wachs et al. [90] applied in situ Raman and XANES (X-ray absorption near-edge structure) study for the characterization of niobia species on oxide supports. At very low surface coverages they found fourfold coordinated surface NbO_4 species characterized by Raman bands at 980–990 cm^{-1} . Intermediate surface coverage led to the formation of fivefold coordinated surface NbO_5 species (Raman bands at 930–950 cm^{-1} range), whereas high surface coverage gave rise to Raman bands at 630–650 cm^{-1} characteristic of sixfold coordinated surface NbO_6 species. Jehng and Wachs [91] reported that terminal Nb=O bonds in Raman spectra occur between 850 and 1000 cm^{-1} and this kind of bond is present in highly distorted octahedral NbO_6 structures. The band due to the Nb–O bond usually appears between 500 and 700 cm^{-1} in Raman spectra and belongs to the slightly distorted octahedral NbO_6 structures [63]. This bond is also present in NbO_7 and NbO_8 species, bringing about at least two bands in the IR spectra. More information about Raman frequencies from niobium oxides depending on lattice parameters is presented in Table 1.

Raman spectroscopy was one of the methods applied to the study of niobia supported on silica and helped in the identification of the surface species formed [74,90]. Antonelli and coworkers [49,50] used Raman spectroscopy for the characterization of C_{60} (fulleride) units in mesoporous niobium and tantalum oxides as well as in K_3C_{60} + Nb-TMS1.

The Raman based methods, i.e., laser Raman spectroscopy (LRS), surface-enhanced Raman scattering (SERS) and the modified IR spectroscopy (IR

Table 1
The relationship between niobium oxide structures and Raman frequencies^a

Symmetry	Type	Raman bands (cm ⁻¹)	Compounds
	NbO ₄	790–830	YNbO ₄
	NbO ₇ and NbO ₈	500–700	Nb ₂ O ₅ (amorphous; TT-, T-H-form), LiNbO ₃ , NaNbO ₃
	NbO ₆	850–1000	Nb ₂ O ₅ (H), AlNbO ₄ , Nb(HC ₂ O ₄) ₅

^a Reproduced from Ref. [91].

reflection absorption spectroscopy, IRRAS) have been used to demonstrate that a stable passivated film can be easily formed on Nb in 0.15 M NaCl [92]. The authors showed the Raman spectra of NbO₂ and Nb₂O₅.

Raman spectra exhibited perhaps the best evidence for the isomorphous substitution of Ti by Nb in the ETS-10 (microporous titanasilicate) framework [93]. ETS-10 gives a main strong and sharp band at ca. 735 cm⁻¹, assigned to the TiO₆ octahedra. With the increase of Nb content this peak shifts slightly and broadens, and simultaneously, a band grows at ca. 664 cm⁻¹ (typical of NbO₆ octahedra in microporous niobosilicates). Similar evidence is shown for NbS-1 zeolite (MFI structure) [94].

Katihar and coworkers [95] showed Raman spectra of Ta₂O₅ recorded at room temperature, and also at low and high temperatures. Moreover, they used Raman scattering to study the phase transition in (Ta₂O₅)_{1-x}(TiO₂)_x from triclinic to monoclinic one [96].

The Raman spectroscopy has been recently applied [88] for the study of bulk tantalum hydrate (Ta₂O₅·*n*H₂O) before and after exposure to different temperatures in air, as well as for the estimation of Ta oxide structure supported on Al₂O₃, TiO₂, ZrO₂, and SiO₂. Tantalum hydrate is amorphous with a characteristic broad Raman band at ~660 cm⁻¹. The heat treatment at 1073 K transforms the amorphous

tantalum hydrate into well crystallized bulk Ta₂O₅ which gives rise to the strongest Raman bands at ~102 and 253 cm⁻¹, two less intensive bands at 621 and 705 cm⁻¹, and some other weak bands at approximately 200, 340, 490, 843, and 944 cm⁻¹. Raman spectroscopy revealed that the supported tantalum oxide phases possess significantly different structure from the bulk Ta₂O₅. The molecular structures of the surface TaO_x species on the different oxide supports primarily possess polymerized TaO₅/TaO₆ coordination with the exception of SiO₂, which contained mostly isolated TaO₄ tetrahedrons.

4.4. IR spectroscopy

The commonly used technique for the characterization of active species on the surface of solids, i.e., the adsorption of “probe molecules” followed by the IR spectroscopy study, has been also applied to the investigation of Nb- and Ta-containing materials. Adsorption of pyridine or lutidine combined with IR measurements was used in the study of Pt/Nb₂O₅/Al₂O₃ [97], Nb/Al₂O₃ [98], NbMCM-41 and Cu–NbMCM-41 [99–102], amorphous niobium phosphate [103]. The adsorption of NO followed by IR study may provide an insight into the redox properties as well as the oxidation state of metal on the solid surface. This method was used for instance in the characterization of Nb₂O₅ and Ta₂O₅ sup-

ported on TiO_2 [104] or in the study of mesoporous molecular sieves (NbMCM-41) [38,59,105]. The adsorption of acetophenone on niobium acid [106] and acetonitrile on niobium phosphate [64] were also applied.

Following the new invention [107,108] of the use of IR bands in the $850\text{--}1000\text{ cm}^{-1}$ region to the characterization of cations in molecular sieves, the localization of Nb in mesoporous molecular sieves (NbMCM-41) has been studied [59]. The Si–O–Si vibrations observed in the $1020\text{--}1100\text{ cm}^{-1}$ range are perturbed in the various manners depending on the location of niobium cations (framework or extra framework) and their interaction with Si–O–Si vibrational mode. The appearance of two IR bands in the transmission window ($850\text{--}1000\text{ cm}^{-1}$) of the NbMCM-41 spectrum indicated the existence of two various Nb-species interacting with T–O–T vibrations (framework NbO^- and Nb^+ species). The identification of Nb in the framework or extra framework positions based on the intensity of the perturbed IR bands after adsorption of NO.

4.5. Electron spin resonance (ESR) study

There is more literature data showing ESR spectra of Nb-containing compounds than that of Ta-containing materials. It is commonly recognized that the paramagnetic species is Nb or Ta with the oxidation state 4+. Little is known about the ESR spectra of Nb(2+) because, as it is described in the literature, they are similar to those observed for Nb(4+) species with d^1 configuration and the two states cannot be distinguished by the ESR technique [109]. No ESR signals of Nb^{4+} in NbO_2 is usually observable due to the diamagnetic property. The ESR signal of Nb^{4+} at the $g = 1.85$ was, however, detected for the niobium oxide of the controlled composition. During the reduction of niobium oxide the O/Nb value decreases. The spin density of Nb^{4+} formed in niobium oxide by the controlled reduction is the highest when $\text{O/Nb} = 2.496$. The further reduction causes the decrease in the spin density and it is due to the magnetic coupling of neighboring Nb^{4+} cations. Only the isolated cation free from the

Table 2

Some other techniques and examples of their application to the characterization of Nb and Ta compounds

Technique	Compound	References
Ultraviolet-visible spectroscopy (UV-Vis) including diffuse reflectance spectroscopy (UV-Vis DRS)	Nb_2O_5 film	[32,116–118]
	Nb_2O_5	[1,117]
	$\text{CeO}_2\text{--Nb}_2\text{O}_5$	[118]
	$\text{Pd/Nb}_2\text{O}_5$	[117]
	$\text{Pt/Nb}_2\text{O}_5$	[97]
	Nb phosphate	[64]
	$\text{Nb}_2\text{O}_5/\text{SiO}_2$	[119]
	NbMCM-41	[119]
	Nb–Cl complexes	[113,120]
	TaS-1 (tantalum silicate)	[24]
	Ta_2O_5	[1]
Extended X-ray absorption fine structure (EXAFS), and XANES	Nb-oxides	[74,90,121]
	Nb foil	[121]
	Nb sulfide	[122–124]
	Pd , $\text{Co/Nb}_2\text{O}_5$	[125]
	Ni , $\text{Co/Al}_2\text{O}_3$ + Nb oxides	[54]
Voltammetry (cyclic and linear sweep)	Nb_2O_5 film	[23,33]
	$\text{NaCl--KCl--K}_2\text{NbF}_3$ and $\text{NaCl--KCl--K}_3\text{NbOF}_6$	[44]
Elipsometry	Nb_2O_5 film	[33]
	Ta_2O_5	[52]

diamagnetic interaction gives the ESR absorption spectrum. Nb^{4+} cations must be well dispersed (isolated from each other) in the non-stoichiometric phase of the T-type structure, resulting in the detection of the ESR absorption [110]. The well isolation of Nb^{4+} cations was reached in niobium oxide on the silica matrix [110]. It was also obtained in the diluted toluene solutions of $\text{NbCl}_2\text{H}_2(\text{dmpe})_2$, where $\text{dmpe} = 1,2\text{-bis}(\text{dimethylphosphino})\text{ethane}$ [111]. Isolated tantalum was reached in the toluene solution of $\text{TaCl}_2\text{H}_2(\text{PMe}_3)_4$ [111]. Hyperfine structure in the ESR spectrum of ^{181}Ta ($I = \frac{7}{2}$, $\sim 100\%$ abundance) gives rise to eight lines observed at room temperature, whereas that of ^{93}Nb ($I = \frac{9}{2}$, $\sim 100\%$ abundance) consists of 10 lines. The ESR spectra were also registered in the toluene solutions of $\text{Nb}_3\text{Cl}_6(t\text{-BuNC})_5$ [109] $\text{Nb}_2\text{Cl}_8\text{PMe}_3$, and $\text{Nb}_2\text{Cl}_8\text{PMe}_2\text{Ph}$ [112] $\text{NbCl}_2(\text{dpm})$, where $\text{Hdpm} = 2,2,6,6\text{-tetramethylheptane-3,5-dione}$ [113]. The dilution of $\text{Nb}(\text{O}_2\text{CNEt}_2)_4$ in toluene led to the registration of 10-line hyperfine pattern in ESR spectrum at room temperature ($g_{\text{iso}} = 1.951$, $A_{\text{iso}} = 160.6\text{ G}$). The same effect was reached when $\text{Nb}(\text{O}_2\text{CNEt}_2)_4$ was diluted in solid $\text{Zr}(\text{O}_2\text{CNEt}_2)_4$ [114].

Prakash and Kevan [94] demonstrated the ESR spectra of γ -irradiated NbS-1 (niobosilicate with MFI zeolite structure) consisting of 10-line hyperfine structure. The ESR spectra of $\text{Nb}(\text{CO})_6$ in solid CO at 2 K and that of $\text{Nb}(\text{N}_2)_6$ in solid N_2 at 4 K are presented in [115].

The examples of other techniques used for the characterization of Nb- and Ta-containing compounds are shown in Table 2.

Acknowledgements

The KBN (Polish Committee for Scientific Research), grant no. 3 T09A 102 19 is acknowledged.

References

- [1] A. Townshend, *Encyclopedia of Analytical Science*, Academic Press, London, 1995, p. 3312.
- [2] A. Townshend, *Encyclopedia of Analytical Science*, Academic Press, London, 1995, p. 5097.
- [3] I. Mori, Y. Fujita, M. Toyoda, S. Kubo, *Fresenius J. Anal. Chem.* 342 (1992) 80.
- [4] N. Vachirapatama, P. Doble, Z. Yu, M. Macka, P.R. Haddad, *Anal. Chim. Acta* 434 (2001) 301.
- [5] G.A. Jenner, H.P. Longrich, S.E. Jackson, B.J. Fryer, *Chem. Geol.* 83 (1990) 133.
- [6] S.M. Eggins, J.D. Woodhead, L.P.J. Kinsley, G.E. Mortimer, P. Sylvester, M.T. McCulloch, J.M. Hergt, M.R. Handler, *Chem. Geol.* 134 (1997) 311.
- [7] P. Roychowdhury, N.K. Roy, A.K. Das, *Atomic Spectrosc.* 16 (1995) 104.
- [8] K. Satyanarayana, M.A. Nayeem, *Atomic Spectrosc.* 14 (1993) 180.
- [9] N. Vachirapatama, M. Macka, B. Paull, C. Munker, P.R. Haddad, *J. Chromatogr. A* 850 (1999) 257.
- [10] N. Vachirapatama, P. Doble, P.R. Haddad, *J. Chromatogr. A* 885 (2000) 369.
- [11] D.M. Antonelli, J.Y. Ying, *Angew. Chem. Int. Ed. Engl.* 35 (1996) 426; D.M. Antonelli, J.Y. Ying, *Chem. Mater.* 8 (1996) 874; D.M. Antonelli, J.Y. Ying, *Curr. Opin. Colloid Interf. Sci.* 1 (1996) 523.
- [12] D.M. Antonelli, A. Nakahira, J.Y. Ying, *Inorg. Chem.* 35 (1996) 3126.
- [13] Q.S. Huo, D.I. Margolese, U. Ciesla, P. Feng, T.E. Gier, P. Sieger, R. Leon, P.M. Petroff, F. Schüth, G.D. Stucky, *Nature* 368 (1994) 317.
- [14] T. Sun, J.Y. Ying, *Nature* 389 (1997) 704; T. Sun, J.Y. Ying, *Angew. Chem. Int. Ed. Engl.* 37 (1998) 664.
- [15] M.A. Bizero, D.L.A. De Faria, V.R.L. Constantino, *J. Mater. Sci.* 37 (2002) 265.
- [16] J. Mendez-Vivar, P. Bosh, V.H. Lara, *J. Sol-Gel Sci. Technol.* 6 (1996) 257.
- [17] H. Kominani, M. Miyakawa, S.-Y. Murakami, T. Yasuda, M. Kohno, S.-I. Onoue, Y. Kera, B. Ohtani, *Phys. Chem. Chem. Phys.* 3 (2001) 2697.
- [18] J.D. Aiken III, R.G. Finke, *J. Mol. Catal. A* 145 (1999) 1.
- [19] J. Gonzales, M.C. del Ruiz, J.B. Rivarola, D. Pasquevich, *J. Mater. Sci.* 33 (1998) 4173.
- [20] P. Nair, J. Nair, A. Raj, K. Maeda, F. Mizukami, T. Okubo, H. Izutsu, *Mater. Res. Bull.* 34 (1999) 225.
- [21] I. Zhitomirsky, *Mater. Lett.* 35 (1998) 188.
- [22] P. Perez, V.A.C. Haanappel, M.F. Stroosnijder, *Mater. Sci. Eng. A* 284 (2000) 126.
- [23] A. Pawlicka, M. Atik, M.A. Aegerter, *Thin Solid Films* 301 (1997) 236.
- [24] Y.S. Ko, W.S. Ahn, *Micropor. Mesopor. Mater.* 30 (1999) 283.
- [25] S.I. Hong, M.A. Hill, *Mater. Sci. Eng. A* 281 (2000) 189.
- [26] M.J. Sayagués, J.L. Hutchison, *J. Solid State Chem.* 124 (1996) 116; M.J. Sayagués, J.L. Hutchison, *J. Solid State Chem.* 146 (1999) 202.
- [27] M.J. Sayagués, J.L. Hutchison, *J. Solid State Chem.* 163 (2002) 137.
- [28] M.J. Sayagués, F. Krumeich, J.L. Hutchison, *Micron* 32 (2001) 457.
- [29] F. Krumeich, J.L. Hutchison, M.J. Sayagués, *Z. Anorg. Allg. Chem.* 625 (1999) 755.

- [30] J. Gonzales, M.C. del Ruiz, D. Pasquevich, A. Bohé, J. Mater. Sci. 36 (2001) 3299.
- [31] M. Schmitt, M.A. Aegerter, *Electrochim. Acta* 46 (2001) 2105.
- [32] K. Kukli, M. Ritala, M. Leskelä, R. Lappalainen, *Chem. Vap. Deposition* 4 (1998) 29.
- [33] N. Özer, D.-G. Chen, C.M. Lampert, *Thin Solid Films* 277 (1996) 162.
- [34] M. Paulis, M. Martin, D.B. Soria, A. Diaz, J.A. Odriozola, M. Montes, *Appl. Catal. A* 180 (1999) 411.
- [35] F.B. Noronha, C.A. Perez, M. Schmal, R. Fréty, *Phys. Chem. Chem. Phys.* 1 (1999) 2861.
- [36] E.B. Pereira, M.M. Pereira, Y.L. Lam, C.A.C. Perez, M. Schmal, *Appl. Catal. A* 197 (2000) 99.
- [37] M. Ziolek, I. Nowak, *Mater. Res. Soc.* (1999) 997.
- [38] M. Ziolek, I. Sobczak, I. Nowak, P. Decyk, J. Stoch, *Stud. Surf. Sci. Catal.* 135 (2001) 151.
- [39] M. Ziolek, I. Nowak, H.G. Karge, *Stud. Surf. Sci. Catal.* 94 (1995) 270.
- [40] V. Gauthier, F. Bernard, E. Gaffet, C. Josse, J.P. Larpin, *Mater. Sci. Eng. A* 272 (1999) 334.
- [41] M. Nagai, R. Nakauchi, Y. Ono, S. Omi, *Catal. Today* 57 (2000) 297.
- [42] S.K. Pradhan, T. Chakraborty, S.P. Sen Gupta, C. Suryanarayana, A. Frefer, F.H. Froes, *NanoStruct. Mater.* 5 (1995) 53.
- [43] A.G. Aleksanyan, S.K. Dolukhanyan, *Int. J. Hydrogen Energy* 26 (2001) 429.
- [44] L.P. Polyakova, T.V. Stogova, E.G. Polyakov, A.V. Arakcheeva, V.V. Grinevich, *Plasma and Ions* 3 (2000) 21.
- [45] S.A. Holmes, J. Al-Saedi, V.V. Gulians, P. Boolchand, D. Georgiev, U. Hackler, E. Sobkow, *Catal. Today* 67 (2001) 403.
- [46] H. Habazaki, K. Hon-yashiki, K. Ito, H. Mitsui, A. Kawashima, K. Asami, K. Hashimoto, S. Mrowec, *Mater. Sci. Eng. A* 267 (1999) 267.
- [47] M. Ziolek, I. Nowak, *Zeolites* 18 (1997) 356.
- [48] M. Ziolek, I. Nowak, H. Poltorak, A. Lewandowska, I. Sobczak, *Stud. Surf. Sci. Catal.* 125 (1999) 691.
- [49] B. Ye, M. Trudeau, D. Antonelli, *Chem. Mater.* 13 (2001) 2730.
- [50] B. Ye, D. Antonelli, *Adv. Mater.* 13 (2001) 29.
- [51] J. Xu, H. Mao, P.M. Bell, *High Temp.–High Press.* 16 (1984) 495.
- [52] E. Franke, M. Schubert, C.L. Trimble, M.J. De Vries, J.A. Woollam, *Thin Solid Films* 388 (2001) 283.
- [53] K. Kukli, M. Ritala, M. Leskelä, *NanoStruct. Mater.* 8 (1997) 785.
- [54] V. Gaborit, N. Allali, Ch. Geantet, M. Breyse, M. Vrinat, M. Danot, *Catal. Today* 57 (2000) 261.
- [55] P.G. Pries de Oliveira, J.G. Eon, M. Chavant, A.S. Riché, V. Martin, S. Caldarelli, J.C. Volta, *Catal. Today* 57 (2000) 177.
- [56] M. Ferroni, M.C. Carotta, V. Guidi, G. Martinelli, F. Ronconi, O. Richard, D. Van Dyck, J. Van Landuyt, *Sensors and Actuators B* 68 (2000) 140.
- [57] J.T. Richardson, *Principles of Catalyst Development*, Plenum Press, New York, 1992, p. 140.
- [58] L.C. Passoni, M.R.H. Siddiqui, A. Steiner, I.V. Kozhevnikov, *J. Mol. Catal. A* 153 (2000) 103.
- [59] M. Ziolek, I. Sobczak, A. Lewandowska, I. Nowak, P. Decyk, M. Renn, B. Jankowska, *Catal. Today* 70 (2001) 169.
- [60] M.M. Pereira, E.B. Pereira, L.Y. Lau, M. Schmal, *Catal. Today* 57 (2000) 291.
- [61] V.R.K. Chary, T. Bhaskar, G. Kishan, R.K. Reddy, *J. Phys. Chem. B* 105 (2001) 4392.
- [62] L.J. Burcham, I.E. Wachs, *Catal. Today* 49 (1999) 467.
- [63] J. Mendez-Vivar, P. Bosh, V.H. Lara, *J. Sol–Gel Sci. Technol.* 6 (1996) 257.
- [64] T. Armaroli, G. Busca, C. Carlini, M. Giuttari, A.M.R. Galletti, G. Sbrana, *J. Mol. Catal. A* 151 (2000) 233.
- [65] M. Zhou, L. Andrews, *J. Phys. Chem. A* 102 (1998) 8251.
- [66] L. Zhang, J.Y. Ying, *AIChE J.* 43 (1997) 2793.
- [67] J.N. Kondo, L. Lu, Y. Takahara, K.-I. Maruya, K. Domen, N. Igarashi, T. Tatsumi, *Bull. Chem. Soc. Jpn.* 73 (2000) 1123.
- [68] H.Y. Chen, L. Chen, J. Lin, K.L. Tan, J. Li, *Inorg. Chem.* 36 (1997) 1417.
- [69] R.K. Rana, B. Viswanathan, *Catal. Lett.* 52 (1998) 25.
- [70] E.-M. El-Malki, R.A. van Santen, W.M.H. Sachtler, *J. Phys. Chem. B* 103 (1999) 4611.
- [71] V.V. Fomichev, *Russ. Chem. Bull.* 43 (1994) 1943.
- [72] Y. Iwasawa, *Tailored Metal Catalyst*, Kluwer, Dordrecht, 1986, p. 9.
- [73] S. Prasad, P. Zhao, J. Huang, J.J. Fitzgerald, J.S. Shore, *Solid State Nucl. Mag. Reson.* 14 (1999) 231.
- [74] Y. Iwasawa, *Stud. Surf. Sci. Catal.* 101 (1996) 21.
- [75] G. Binning, H. Rohrer, C. Gerber, E. Weibel, *Phys. Rev. Lett.* 49 (1982) 57.
- [76] Y. Uehara, T. Fujita, M. Iwami, S. Ushioda, *Surf. Sci.* 472 (2001) 59.
- [77] A. Daccà, G. Gemme, L. Mattera, R. Parodi, *Appl. Surf. Sci.* 126 (1998) 219.
- [78] K. Sugiyama, G. Anan, T. Shimada, T. Ohkoshi, T. Ushikubo, *Surf. Coat. Technol.* 112 (1999) 76.
- [79] M.Z. Atashbar, H.T. Sun, B. Gong, W. Wlodarski, R. Lamb, *Thin Solid Films* 326 (1998) 238.
- [80] M. Vettrano, M. Trudeau, D.M. Antonelli, *Inorg. Chem.* 40 (2001) 2088.
- [81] V. Pârvulescu, V.I. Pârvulescu, P. Grange, *Catal. Today* 57 (2000) 193.
- [82] V.L.S. Teixeira da Silva, M. Schmal, S.T. Oyama, *J. Solid State Chem.* 123 (1996) 168.
- [83] W.L. Manner, J.A. Lloyd, R.J. Hanrahan Jr., M.T. Paffett, *Appl. Surf. Sci.* 150 (1999) 73.
- [84] R. Hofer, M. Textor, N.D. Spencer, *Langmuir* 17 (2001) 4014.
- [85] B. Schneider, R. Niemann, Ch. Kuper, H. Hesse, M. Neumann, *J. Electron Spectrosc. Relat. Phenom.* 96 (1998) 37.
- [86] K. Tabaka, M. Kamada, T. Choso, H. Munakata, *J. Phys. Chem. B* 101 (1997) 9161.
- [87] K. Teruuchi, H. Habazaki, A. Kawashima, K. Asami, K. Hashimoto, *Appl. Catal.* 76 (1991) 79.
- [88] Y. Chen, J.L.G. Fierro, T. Tanaka, I.E. Wachs, submitted to *J. Phys. Chem. B*.

- [89] J. Stencel, *Raman Spectroscopy for Catalysis*, Kluwer Academic Publishers, Dordrecht, 1989, p. 1.
- [90] I.E. Wachs, J.-M. Jehng, G. Deo, H. Hu, N. Arora, *Catal. Today* 28 (1996) 199.
- [91] J.-M. Jehng, I.E. Wachs, *Catal. Today* 8 (1990) 37; J.-M. Jehng, I.E. Wachs, *J. Phys. Chem.* 95 (1991) 7373.
- [92] B.X. Huang, K. Wang, J.S. Church, Y.-S. Li, *Electrochim. Acta* 44 (1999) 2571.
- [93] J. Rocha, P. Brandão, J.D. Pedrosa de Jesus, A. Philippou, M.W. Anderson, *J. Chem. Soc., Chem. Commun.* (1999) 471.
- [94] A.M. Prakash, L. Kevan, *J. Am. Chem. Soc.* 120 (1998) 13148.
- [95] P.S. Dobal, R.S. Katiyar, Y. Jiang, R. Guo, A.S. Bhalla, *J. Raman Spectrosc.* 31 (2000) 1061.
- [96] P.S. Dobal, R.S. Katiyar, Y. Jiang, R. Guo, A.S. Bhalla, *J. Phys. Chem. Solids* 61 (2000) 1805.
- [97] F.B. Passos, A.G. Aranda, R.R. Soares, M. Schmal, *Catal. Today* 43 (1998) 3.
- [98] C.L.T. Da Silva, V.L.L. Comorim, J.L. Zotin, M.L.R.D. Pereira, A. da Costa Faro Jr., *Catal. Today* 57 (2000) 209.
- [99] M. Ziolek, I. Nowak, J.C. Lavalley, *Catal. Lett.* 45 (1997) 259.
- [100] M. Ziolek, I. Nowak, P. Decyk, O. Saur, J.C. Lavalley, *Mater. Res. Soc.* (1999) 833.
- [101] M. Ziolek, I. Nowak, I. Sobczak, A. Lewandowska, P. Decyk, J. Kujawa, *Stud. Surf. Sci. Catal.* 129 (2000) 813.
- [102] M. Ziolek, I. Sobczak, I. Nowak, M. Daturi, J.C. Lavalley, *Appl. Catal. B* 28 (2000) 197.
- [103] J.C.G. Da Silva, S. Folgueras-Domínguez, A.C.B. Dos Santos, *J. Mater. Sci. Lett.* 18 (1999) 197.
- [104] M. Kudo, T. Kosaka, Y. Takahashi, H. Kokusen, N. Sotani, S. Hasegawa, *Sensors and Actuators B* 69 (2000) 10.
- [105] M. Ziolek, I. Sobczak, I. Nowak, M. Daturi, J.C. Lavalley, *Top. Catal.* 11 (2000) 343.
- [106] I. Ahmad, T.J. Dines, J.A. Anderson, C.H. Rochester, *Spectrochim. Acta A* 55 (1999) 397.
- [107] Z. Sobalik, Z. Tvaruzkova, B. Wichterlova, *J. Phys. Chem. B* 102 (1998) 1077.
- [108] Z. Sobalik, J. Dedecek, I. Ikonnikov, B. Wichterlova, *Micropor. Mesopor. Mater.* 21 (1998) 525.
- [109] F.A. Cotton, W.J. Roth, *Inorg. Chim. Acta* 126 (1987) 161.
- [110] Y. Wada, A. Morikawa, *Catal. Today* 8 (1990) 13.
- [111] M.L. Luetkens Jr., W.L. Elcesser, J.C. Huffmam, A.P. Sattelberger, *Inorg. Chem.* 23 (1984) 1718.
- [112] F.A. Cotton, S.A. Duraj, W.J. Roth, *Inorg. Chem.* 23 (1984) 3592.
- [113] F.A. Cotton, M.P. Diebold, W.J. Roth, *Polyhedron* 4 (1985) 1485.
- [114] F. Calderazzo, U. Englert, C. Maichle-Mössmer, F. Marchetti, G. Pampaloni, D. Petroni, C. Pinzino, J. Strähle, G. Tripepi, *Inorg. Chim. Acta* 270 (1998) 177.
- [115] S.H. Parrish, R.J. Van Zee, W. Weltner Jr., *J. Phys. Chem. A* 103 (1999) 1025.
- [116] M.G. Krishna, A.K. Bhattacharya, *Mater. Sci. Eng. B* 86 (2000) 41.
- [117] R. Brayner, G. Viau, G.M. da Cruz, F. Fiévet-Vincent, F. Fiévet, F. Bozon-Verduaz, *Catal. Today* 57 (2000) 187.
- [118] R. Brayner, D. Ciuparu, G.M. da Cruz, F. Fiévet-Vincent, F. Bozon-Verduaz, *Catal. Today* 57 (2000) 261.
- [119] X.T. Gao, I.E. Wachs, M.S. Wong, J.Y. Ying, *J. Catal.* 203 (2001) 18.
- [120] M. Bachtler, J. Rockenberger, W. Freyland, Chr. Rosenkilde, T. Ostvold, *J. Phys. Chem.* 98 (1994) 742.
- [121] F. D'Acapito, S. Mobilio, P. Cikmacs, V. Merlo, I. Davoli, *Surf. Sci.* 468 (2000) 77.
- [122] N. Allali, A. Yacoubi, A. Nadiri, C. Geantet, M. Danot, *Ann. Chim. Sci. Mater.* 23 (1998) 209.
- [123] N. Allali, A. Leblanc, M. Danot, Ch. Geantet, M. Vrinat, M. Breysse, in: G. Centi, et al. (Eds.), *Environmental Catalysis*, SCI Publishers, Rome, Italy, 1995, p. 93.; N. Allali, A. Leblanc, M. Danot, Ch. Geantet, M. Vrinat, M. Breysse, *Catal. Today* 27 (1996) 137.
- [124] N. Allali, E. Prouzet, A. Michalowicz, V. Gaborir, A. Nadiri, M. Danot, *Appl. Catal. A* 159 (1997) 333.
- [125] F.B. Noronha, M. Schmal, B. Moraweck, P. Delichere, M. Brun, F. Villain, R. Frety, *J. Phys. Chem. B* 104 (2000) 5478.